




# Nature-inspired three-dimensional foam-like porous carbon surface modified separator for high-performance Li-S batteries

Krishnan Vignesh<sup>a</sup>, Tamilarasan Mathivanan<sup>a</sup>, Mariappan Ganeshbabu<sup>a</sup>,  
Nuthalapati Prasanna Naga Puneeth<sup>a</sup>, Balasubramaniam Ramkumar<sup>b</sup>, Yun Sung Lee<sup>b</sup>,  
Ramakrishnan Kalai Selvan<sup>a,\*</sup> 

<sup>a</sup> Energy Storage and Conversion Devices Laboratory, Department of Physics, Bharathiar University, Coimbatore 641046, Tamil Nadu, India

<sup>b</sup> Faculty of Chemical Engineering, Chonnam National University, Gwangju 500-757, South Korea

## ARTICLE INFO

### Keywords:

Lichens  
Porous carbon  
Modified separators  
Li-S batteries

## ABSTRACT

The increasing growth of electric vehicles and portable electronics has led to a surplus energy demand in recent decades. Lithium-sulfur (Li-S) batteries have garnered significant attention and are believed to be the most promising future for sustainable high energy supply. Despite their high theoretical capacity, polysulfide shuttling has been a thorny drawback for their experimental performance degradation. In this work, lichen (*Parmotrema stippeum*), a unique species with a mutualistic symbiotic relationship with fungi and algae, was used as a biomass for carbon precursor to modify the glass fiber (GF) separator. The necessary 3-dimensional porous carbon structure and active surface functional groups are obtained without extra additives. The porous network associated with L-600 accompanies foam-like structures that are anticipated to filter up polysulfides and facilitate lithium ions transport in the electrode-electrolyte interface. Thereby, the porous architecture ensures physical sites and traps dissolved polysulfide intermediate compounds, holding them as potential active materials that can undergo catalytic reactions within the cathode side. The Li-S cell, accompanied by the modified separator (L-600), offered a high initial specific capacity of 1330 mAh g<sup>-1</sup> at 0.2 C. Further, the Li-S cell offered a prolonged reversible capacity of 725 mAh g<sup>-1</sup> after 200 cycles, with a capacity degradation rate of 0.22 % per cycle. Post-stability analysis of the Li-S separator confirms the effectiveness of the modified separator in mitigating polysulfide shuttling.

## 1. Introduction

Lithium-sulfur (Li-S) batteries, since their big breakthrough in 2009 (mesoporous carbon composites for high capacity), have attracted wide attention towards the new era of energy storage devices [1–3]. Lithium is the lightest, least dense alkaline metal (about 0.534 g/cm<sup>3</sup>), with the highest tendency to lose its unpaired single electron in the outer shell, resulting in the electrochemical potential value of about −3.04 V vs. SHE [4,5]. These properties resulted in delivering high energy density, and they became a valuable electrode for Li-ion batteries. The lithium was paired with several intercalation-type cathodes like LiCoO<sub>2</sub>, LiMn<sub>2</sub>O<sub>4</sub>, and LiFePO<sub>4</sub> to increase the specific capacities [6]. However, the outcomes are insufficient to supply the demand of future needs. Therefore, Li-S batteries evolved as a potential energy-storing candidate due to their high energy density, improved safety, and economically

viable raw materials [7].

Sulfur is the 16<sup>th</sup> most abundant and an electrochemically active element; it can readily accept up to two electrons per atom during the electrochemical process at ~2.10 V vs. Li/Li<sup>+</sup>. Unlike conventional insertion cathode materials, the critical aspect of sulfur is that it undergoes distinct compositional, morphological, and structural changes during charging and discharging cycling [8]. These changes are associated with long-chain soluble higher-order lithium polysulfides and insoluble lower-order lithium polysulfides [9]. The reduction of higher-order polysulfides to lower-order is accompanied by a series of solid-liquid-solid phase changes during the conversion process [3,10]. Despite the researcher's momentous progress on rechargeable Li-S batteries in the last decade, their commercialization has been a considerable challenge due to poor cyclic stability, highly corrosive lithium, poor conductivity of sulfur, deformation of active material due to expansion,

\* Corresponding author.

E-mail address: [selvankram@buc.edu.in](mailto:selvankram@buc.edu.in) (R. Kalai Selvan).

<https://doi.org/10.1016/j.cartre.2025.100545>

Received 4 January 2025; Received in revised form 30 June 2025; Accepted 1 July 2025

Available online 2 July 2025

2667-0569/© 2025 The Authors. Published by Elsevier Ltd. This is an open access article under the CC BY-NC-ND license (<http://creativecommons.org/licenses/by-nc-nd/4.0/>).

and polysulfide shuttle effect [11].

Several studies reported the enhanced performance of Li-S batteries by modifying the sulfur cathode, additive-based electrolyte, lithium anode modification, and separator redesign [12]. But, commercial battery separators such as single-layered polypropylene (PP), polyethylene (PE), and multi-layered PP/PE/PP fused composite separators and glass fiber (GF) are incapable of supporting polysulfide shuttling and wettability [13]. Also, these separators are comparatively less ionic conductive, and their pore size is immense, which cannot favor repeated cycles in Li-S batteries [14]. GF is the most generally used separator, as it is hydrophilic and highly capable of insulating the electrodes. However, commercial pristine GF separators could not capture the dissolved polysulfides in the electrolyte, causing the shuttle effect. Modifying the surface of the separator is one fruitful method associated with coating functional layers, which can capture the polysulfides and readily support ionic diffusion through the electrodes [15]. Furthermore, it reduces the loss of active material (sulfur), limits the volume expansion of the cathode, and suppresses dendrite formation in the lithium metal anode.

Different coating substances have been reported with unique features, such as carbon-based materials, polymers, transition metal oxides, sulfides, nitrides, phosphides, etc. [16–18]. The carbonaceous materials derived from biomass were employed in Li-S batteries due to their high conductivity, outstanding electrocatalytic properties, tunable porous structures, and good thermal stability [19,20]. Jiang et al. reported a honeycomb-like hierarchical porous carbon for separator modification from lotus seed-based biomass precursor. Zhu et al. reported an eco-friendly carbon aerogel obtained from a sweet potato for a separator-modified Li-S battery with a high initial capacity of 1387 mAh g<sup>-1</sup> (0.2 C) and 1216 mAh g<sup>-1</sup> (0.1 C), respectively [21,22]. Sultanvo et al. synthesized layered porous carbon with NiO-based nanocomposites and achieved an initial specific capacity of 1519 mAh g<sup>-1</sup> (0.2 C) [8]. Nature-inspired architectures, such as hierarchical porous structures, fibrous networks, sponge-like structures, tubular structures, and honeycomb networks, attract more interest in designing and decorating commercial separators [23]. These architects mimic the efficient transport pathways and enable effective electrochemical performance through unique charge/discharge mechanisms [24]. Therefore, combining biomass-derived porous carbon and a commercialized separator is an effective and eco-friendly technique that can chemically and physically trap polysulfides by enabling a synergistic effect.

The algae-based biomass precursors are rich in amino acids, proteins, phospholipids, etc., which is favorable for synthesizing porous carbon associated with *in-situ* heteroatom functionalities [25,26]. Chlorella, Schizochytrium sp., and red algae-derived carbon materials have been successfully synthesized and used in separators to enhance the electrochemical performance of Li-S batteries [27,28]. Chlorella-based biomass-derived porous activated carbon synthesized via NaHCO<sub>3</sub> activation has demonstrated effective lithium polysulfide (LiPS) trapping and dendrite suppression, improving cycling stability and reducing capacity fade. Similarly, Schizochytrium sp.-derived nitrogen-doped porous carbon microspheres have shown high sulfur loading capacity and excellent polysulfide confinement, leading to superior capacity retention and rate performance [29]. The use of carrageenan, a red algae-derived polysaccharide binder, has further enhanced separator performance by chemically binding to sulfur-active material and effectively trapping short-chain polysulfides, enabling a 69.1 % capacity retention after 1000 cycles at 4C [30]. These advancements highlight the potential of algae-derived carbon materials as cost-effective, renewable, and environmentally friendly solutions for mitigating the polysulfide shuttle effect and improving the long-term stability of Li-S batteries.

One such mutualistic symbiotic species is lichen, a composite organism formed through a symbiotic association between a fungus and a photosynthetic partner (typically a green algae). Lichen-based carbon, derived from lichen biomass, has been explored as a potential material for supercapacitors [31]. The lichen-based extract is found to have

plentiful functional groups with polysaccharides, secondary metabolites, and organic acids, such as lichesterinic acid, protocetraric acid, protolichesterinic acid, fumarprotocetraric acid, etc., resulting in hydroxyl groups, silanol groups, and other electroactive species on the surface of porous carbon [32,33]. Importantly, these chemically activated porous carbon structures can effectively trap the polysulfide species with their active functional groups on their surface, and these interlayers can improve the wettability at the separator electrolyte interface. Also, heteroatom functionalities such as N, O, and Si can initiate catalytic activities via strong chemical adsorption, thereby increasing the reversibility of polysulfide species for prolonged cycle life.

This work used biomass Lichen (*Parmotrema stuppeum*) as a carbon precursor to modify the commercial glass fiber (GF) separator. *Parmotrema stuppeum* is a unique species with active functional groups associated with its natural chemical composition and sheet-like morphology, which is highly motivated to utilize these creatures as carbon precursors to achieve prominent sheet-like porous structures. As a result, the 3-D porous network synthesized from the lichens delivered a significant specific capacity of 1330 mAh g<sup>-1</sup> and better cyclic stability. The obtained significant electrochemical performance is due to the porous network, complex functional groups, and high surface area associated with biomass-derived carbon. These fascinating features resulted in an effective polysulfide shuttling effect and enhanced catalytic activity in the cathode separator interface, thereby preventing dendrite formation, inducing polysulfide reversible reactions, and reducing the loss of active material utilization.

## 2. Experimental methods and materials

### 2.1. Preparation of biomass carbon

Lichens collected from the estate region in the hills of the Nilgiris district (11°26'45.1"N and 76°47'37.7" E) are washed in de-ionized water, followed by soaking for 48 h. The washed sample is dried and calcined at three different temperatures of 500 °C, 600 °C, and 700 °C, at a heating rate of 5 °C per minute in a nitrogen atmosphere. After carbonization, the carbon is subjected to two phases of acid treatment with 5 M HCl and 1 M HCl, respectively. The acid-treated sample is washed with DI water several times for neutralization. The wet biomass carbon (BMC) is dried at 85 °C for 24 h, and the dried BMC is ground well. The samples synthesized at three different temperatures are labeled as L-X, where 'L' denotes the precursor Lichen and 'X' denotes its carbonization temperatures of 500, 600, and 700 °C, respectively.

### 2.2. Preparation of BMC-modified separator

A mixture of well-ground BMC carbon, conductive carbon (carbon black), and PVDF (polyvinylidene difluoride) is taken in the ratio of 7:2:1. The mixture is allowed to disperse in the solvent N-Methyl-2-pyrrolidone (NMP). The solution is sonicated for 12 h. After sonication, the slurry is uniformly coated in the glass fiber (GF) separator using the drop-casting method. The surface-modified separator is dried in a vacuum for 48 h. As a result, the homogenous L-X coated GF separator was obtained.

### 2.3. Electrode preparation

The CR-2032 coin cell is constructed to analyze the electrochemical characteristics of the modified GF separators for Li-S battery applications. The Li-S battery consists of a lithium metal anode, sulfur cathode, and commercial separator glass fibers (GF). Lithium metal is clipped to the cell diameter and taken as an anode material. A mixture of sulfur and conductive carbon (carbon black) is taken along with the solvent N-Methyl-2-pyrrolidone (NMP) [34]. The slurry is coated on the aluminium foil and taken as a cathode. The 2032-type coin cells were

assembled using the sulfur cathode, Li metal as the counter electrode (anode), and porous carbon-modified GF as the separator. The electrolyte used was 1 M bis (trifluoromethyl sulfonamide) lithium (LiTFSI) and 0.1 M lithium nitrate ( $\text{LiNO}_3$ ) in a mixture of 1,3-dioxolane (DOL) and 1,2-dimethoxyethane (DME) (1:1 by volume) [35].

## 2.4. Instrumentation

The as-prepared carbon powders were characterized using the Powder X-ray Diffractometer (XRD, Bruker D8 Advance) at a  $0.02^\circ$  step size in the  $2\theta = 10\text{--}80^\circ$ . FTIR analysis was conducted using a JASCO 4100LE. Raman Spectral data were obtained using a JASCO NRS-5100 series confocal Raman Microscope. The surface area was calculated using the Brunauer-Emmett-Teller (BET) method, and pore size distribution was determined using the Barrett-Joyner-Halenda (BJH) method. The X-ray photoelectron spectrometer (XPS Axis Ultra, Kratos Analytical, UK) with monochromatized  $\text{Al K}\alpha$  ( $h\nu = 1486.6$  eV) was utilized to determine the surface compositions of the prepared carbon. Morphological analysis was conducted using FESEM with a CARL ZEISS-SIGMA 300 microscope to determine the particle size and elemental composition. The electrochemical analysis was conducted using a WonAtech battery analyzer in the potential range of 1.6 to 2.8 V vs.  $\text{Li/Li}^+$ . The electrochemical impedance spectra (EIS) were measured from Biologic SP150 in the frequency range of 1 MHz to 10 mHz at an OCV with an amplitude of 10 mV.

## 3. Results and discussion

### 3.1. Physicochemical characterization

The X-ray diffraction patterns of as-prepared L-500, L-600, and L-700 are shown in Fig. 1(a), whose broad peak centered around  $18^\circ$  to  $25^\circ$  and  $42^\circ$  corresponds to (002) and (100) planes of carbon. Distinctly, well-defined prominent peaks over  $26^\circ$  attributed to graphitic platelets owing to the structure of sheet-like precursor (Lichens) [36]. In addition, the peak over  $28^\circ$  corresponds to Si nanoparticles being present naturally in the precursor as an *in-situ* chemical composite [37,38]. However, these silicon particles are known to enhance the electrochemical characteristics through catalytic behavior, which is an added advantage of employing lichens as biomass precursors. The empirical parameter (R-factor) was calculated for L-500, L-600, and L-700 as 2.12, 1.74, and 1.80, respectively. Comparatively, a lower R-value of L-600 suggests that the degree of graphitization has increased compared to the other two samples. The Raman spectra were analyzed to validate the structural defects in the carbon matrix and are given in Figure 1(b). The graphitic peak intensity ( $I_G$ ) at  $1630\text{ cm}^{-1}$  dominates over the defect band intensity ( $I_D$ ) at  $1300\text{ cm}^{-1}$  for all three samples. The D band is associated with the  $A_{1g}$  phonon mode vibrations originating from disordered  $\text{sp}^3$ -hybridized carbon regions. In contrast, the G band arises

from the  $E_{2g}$  phonon mode vibrations, characteristic of the graphitic  $\text{sp}^2$ -hybridized carbon domains in crystalline graphene, as observed in first-order Raman scattering [39]. The  $I_D/I_G$  ratios of L-500, L-600, and L-700 are 0.96, 0.92, and 0.98, respectively. Comparatively, a lower  $I_D/I_G$  ratio of L-600 and a prominent 2D band at  $2900\text{ cm}^{-1}$  suggest that graphitization has improved in the carbon matrix, which can enhance conductivity by improving electrolyte and ionic diffusion [40]. The unique structure observed suggests that  $600^\circ\text{C}$  is an optimal temperature where the balance between disorder and graphitization is achieved. The obtained FTIR spectra of L-500, L-600, and L-700 (Fig. 1(c)) were complex due to diverse functional groups on the activated carbon surface. The peak at  $3436\text{ cm}^{-1}$  indicates the existence of a free and inter-molecular bonded silanol Si-OH group [41]. The peak observed at  $2922\text{ cm}^{-1}$  can be assigned to the C-H group, and the peak at  $1377\text{ cm}^{-1}$  represents the C-H bond group, and  $1078\text{ cm}^{-1}$  represents the stretching of the C-O group [42]. These functional groups detected on the surface of the as-prepared biomass carbon samples can actively participate in the polysulfide trapping by inhibiting their migration and significantly reducing the shuttle effect [43].

The elemental composition was obtained from XPS analysis (Fig. 2(a)), where the survey spectra of all three samples suggest the presence of carbon (C 1s) and oxygen (O 1s) at the binding energies of 285 and 352 eV, respectively. In addition, a trace amount of nitrogen (N 1s) and silicon peak (Si 2p) was also observed at 398 and 100 eV, respectively [44]. From the core-level spectra of C 1s (Fig. 2(b)), the major peak around 284.7 eV corresponds to C-C, and the peaks around 286.4 and 288.4 eV correspond to C-O and C=O, respectively. From the deconvoluted spectra of O 1s (Fig. 2(c)), the peaks centered at 529.5, 531.9, and 534.8 eV correspond to C-O (carboxyl group), -O-, and C=O, respectively [45]. The nitrogen (N 1s) (Fig. 2(d)) and silicon (Si 2p) (Fig. 2(e)) functional groups were also found from the core level spectra with pyridinic-N, pyrrolic-N and graphitic-N at 399.9, 398.2 and 401.8 eV, and Si-C bond at 102.5 eV respectively [46]. These additional functional groups present in L-600 can initiate catalytic reactions, increasing the cyclability of polysulfides in the separator and cathode interface [47]. Fig. 2(f) shows the  $\text{N}_2$  adsorption-desorption profile of the representative L-600 sample, suggesting that the type IV isotherm suggests a uniform and hierarchical porous network. In addition, the porous distribution was derived from the BET analysis as shown in the inset of Fig. 2(f), and the specific surface area of L-600 was found to be  $720\text{ m}^2\text{ g}^{-1}$ . The average pore size was distributed over 1 to 10 nm and 10 to 50 nm, corresponding to micro- and macropores. Macropores facilitate the permeation of the electrolyte and efficient lithium-ion transport. In contrast, the micropores provide many trapping sites for lithium polysulfides, inhibiting their migration between the electrodes [48]. Generally, lithium polysulfide species ( $\text{Li}_2\text{S}_x$ , where  $4 \leq x \leq 8$ ) typically have molecular dimensions in the range of  $\sim 0.5\text{--}1.5$  nm. The microporous framework of L-600 is well-suited to trap these species physically, thereby mitigating their diffusion and suppressing the shuttle

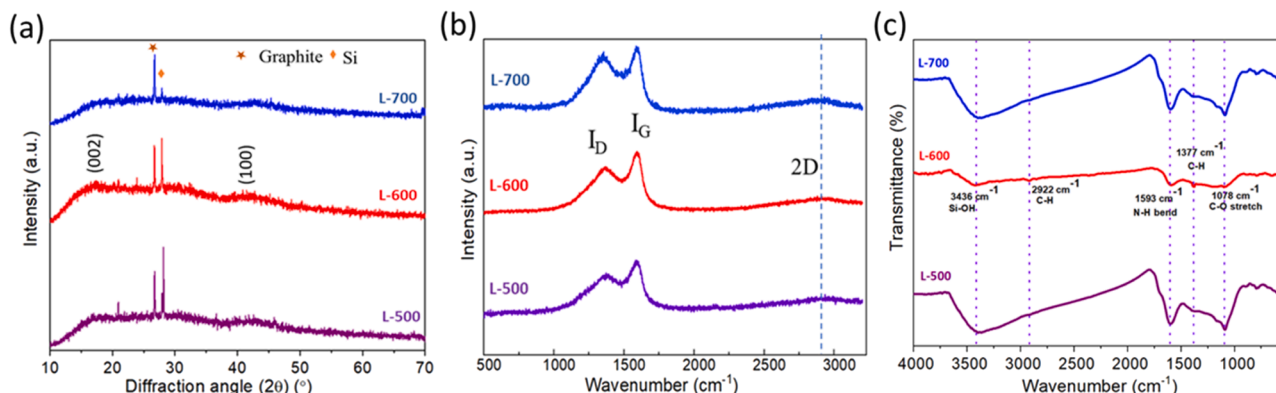
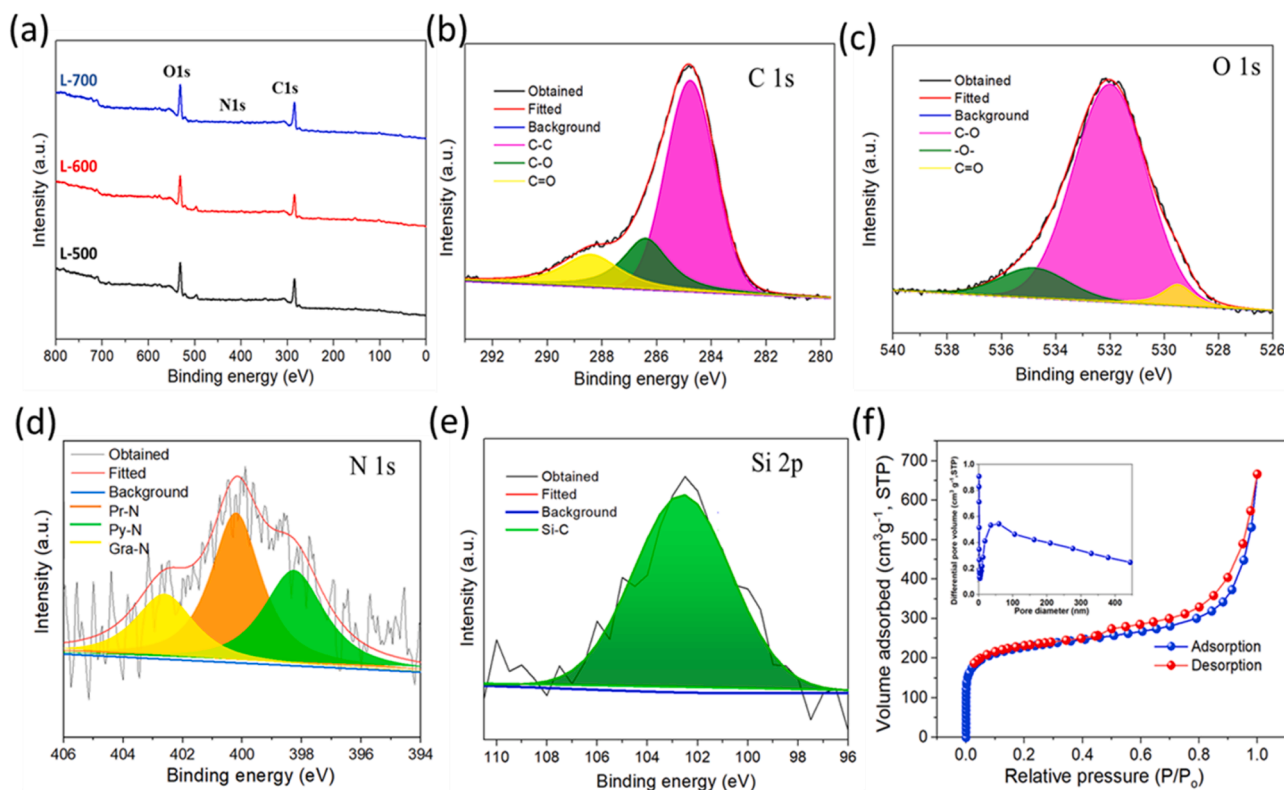


Fig. 1. (a) XRD pattern, (b) Raman spectra, and (c) FTIR spectra of synthesized porous carbon (L-X).





**Fig. 2.** (a) XPS survey spectra of L-X, the deconvoluted spectra of (b) carbon (C 1 s), (c) oxygen (O 1 s), (d) nitrogen (N 1 s), and (e) silicon (Si 2p) of L-600. (f) BET adsorption-desorption isotherm of L-600 (inset: pore size distribution plot).

effect [49].

The morphology of prepared samples L-500, L-600, and L-700 is studied using FESEM images as shown in Fig. 3 (a-c), respectively. The uniform distribution of homogenous pores associated with L-600 will enhance electrochemical performance. The corresponding FESEM images of L-600 at different magnifications are shown in Fig. 3 (d-f), picturing the carbon platelets with well-defined pores distributed over the surface, suggesting a foam-like 3-dimensional (3D) porous carbon network [50,51]. This 3D porous structure is particularly promising in

improving capacity and rate performance, owing to the 3D interconnected carbons providing an extensive interface with the electrolytes for ion interaction reactions [52]. Therefore, this unique morphology may prompt electrolyte penetration with enhanced wettability and ease of lithium-ion transfer in the electrode-electrolyte interface. In contrast, L-500 did not exhibit appreciable porosity, which may be attributed to the lower temperature for complete activation. On the other hand, L-700 also shows well-defined porosity as L-600, suggesting that the sample was well activated at a temperature above 500 °C.

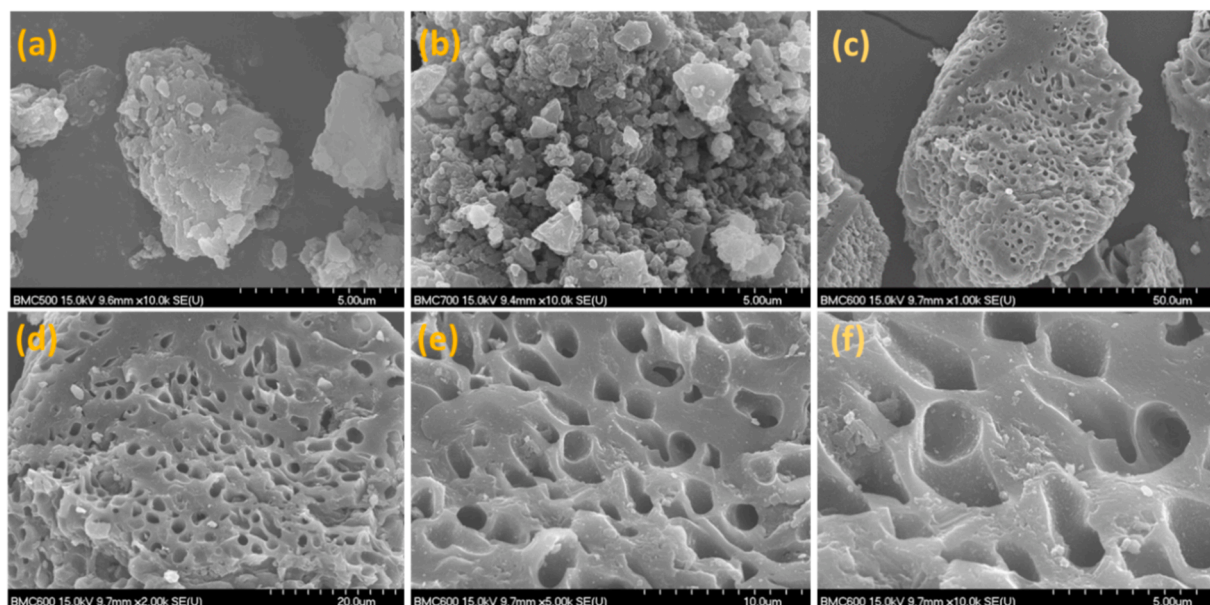


**Fig. 3.** (a-c) FESEM images of L-500, 600, and 700 (d-f) L-600 at different magnifications.



Furthermore, the high-resolution transmission electron microscopic (HRTEM) image, selected area electron diffraction (SAED) pattern, and Energy dispersive spectra (EDS) analyses of the lichen-derived carbon (L-600 sample) are shown in Fig. 4 (a-f), highlighting its nanostructured features and elemental composition. The low-magnification TEM images in Fig. 4 (a-c) at increasing magnifications ( $25,000\times$  to  $100,000\times$ ) reveal a sheet-like morphology with loosely packed, interconnected carbonaceous layers. Fig. 4 (d-e) presents the HRTEM image, which clearly shows lattice fringes with interplanar spacings of 0.317 nm and 0.247 nm, corresponding to the (111) plane of silicon (Si) and the (002) plane of graphitic carbon, respectively. This indicates the coexistence of both carbon and silicon domains, forming a naturally embedded Si and C composite. The SAED pattern in Fig. 4(f) further supports this, with diffraction rings indexed to the (002) and (111) planes, matching the crystalline reflections of graphitic carbon and silicon. The presence of these rings indicates partial crystallinity within the otherwise disordered carbon matrix. Finally, Figure S1 shows the energy-dispersive X-ray spectroscopy (EDS) spectrum, confirming the sample's elemental composition. The strong peaks for C, O, and Si reaffirm the presence of carbonaceous content with embedded silicon nanoparticles. The Cu signal arises from the TEM grid. The observation of Si, supported by both XRD and EDS, suggests that silicon is inherently present in the lichen precursor, making the L-600 sample a unique in-situ Si-C composite. Therefore, from the combined physicochemical analysis of L-500, L-600, and L-700 samples, the L-600 sample is anticipated to offer significant electrochemical performance.

### 3.2. Electrochemical characterization

The electrochemistry of Li-S cells is initiated by performing cyclic voltammetry to study the oxidation and reduction reactions using L-500, L-600, and L-700 modified GF separators. The potential window was optimized as 1.6 to 2.8 V vs. Li/Li<sup>+</sup> with 1.2 V of working voltage at a scan rate of 0.5 mV s<sup>-1</sup>, as shown in Fig. 5(a). The oxidation and reduction peaks of Li-S batteries with modified separators align perfectly with prominent reversibility. L-600 shows a much higher current than L-500 and L-700, with two prominent peaks in the cathodic reduction process attributed to the rapid conversion of higher-order polysulfides that are highly soluble (Li<sub>2</sub>S<sub>x</sub>, 4 ≤ x ≤ 8) and slow reduction of insoluble lower-order polysulfides (Li<sub>2</sub>S<sub>x</sub>, 2 ≤ x ≤ 4) produced from sulfur cathode centered at 2.3 V and 1.9 V respectively [53]. During anodic oxidation,

the lower-order polysulfides are reformed to sulfur, evident from the highly intense anodic peak at 2.6 V vs. Li/Li<sup>+</sup>. The peak current is related to the kinetics of the reaction; a higher peak current suggests faster reaction kinetics. Comparatively, the broad peak of L-500 and L-700 indicates that the sample offers slightly sluggish kinetics. CV analysis shows that the L-600 sample can perform better due to the surface functional groups and uniform porous morphology.

Galvanostatic charge-discharge (GCD) analysis of the Li-S cell was carried out for all three samples coated with a GF separator at a current rate of 0.2 C, in the voltage window of 1.6 V to 2.8 V vs. Li/Li<sup>+</sup> as shown in Fig. 5(b) [54]. Typically, two continuous plateaus corresponding to the reduction of octahedral (S<sub>8</sub>) to higher order and lower order polysulfides were well defined as follows [55]. The initial short plateau at 2.3 V vs. Li/Li<sup>+</sup> corresponds to the higher-order polysulfides, and the comparatively long plateau at 2.05 vs. Li/Li<sup>+</sup> is attributed to the formation of lower-order polysulfides. Similarly, the continuous plateau at oxidation suggests the uninterrupted conversion of lower-order polysulfides Li<sub>2</sub>S<sub>2</sub>/Li<sub>2</sub>S into higher-order polysulfides, and finally, sulfur (S<sub>8</sub>) at the end of oxidation suggests a reversible reaction, which is in good agreement with the CV curve [56]. The performance of specific capacity is calculated from GCD analysis of L-500, L-600, and L-700 @ 0.2 C rate, and their capacity value was found to be 829 mAh g<sup>-1</sup>, 1300 mAh g<sup>-1</sup>, and 476 mAh g<sup>-1</sup>, respectively. Comparatively, L-600 shows better specific capacity owing to its uniform porosity and complex functional groups associated with the carbon matrix. In addition, the L-600 modified separator attains a significant discharge-specific capacity in both the high-voltage region (Q<sub>H</sub>) and low-voltage region (Q<sub>L</sub>) compared to the L-500 and L-700 modified separators. The primary reason for the increased Q<sub>H</sub> and Q<sub>L</sub> is the relieved shuttle effect. The more negligible charge /discharge voltage difference of L-600 of ΔE=0.20 V expresses the reduced polarization. The comparative values of Q<sub>H</sub>, Q<sub>L</sub>, and ΔE are included in Table S1 [57]. Fig. 5(c) shows the stability analysis of L-500, L-600, and L-700 at a 0.2 C rate for 200 cycles. Among these, L-600 shows better stability with 65 % capacity retention after 100 cycles and 55 % retention after 200 cycles. In contrast, L-500 and L-700 samples offered poor stability with < 10 % and 47 % capacity retention after 200 cycles. The stability comparison of the L-600 @GF and pristine GF separator is shown in Figure S2. From Fig. 5(d), the CV curve of the initial five cycles for L-600 overlaps well with its anodic and cathodic peak difference of 0.545 V, indicating good stability of redox reactions, and their location exhibits an extremely stable tendency with the increase in CV cycles.

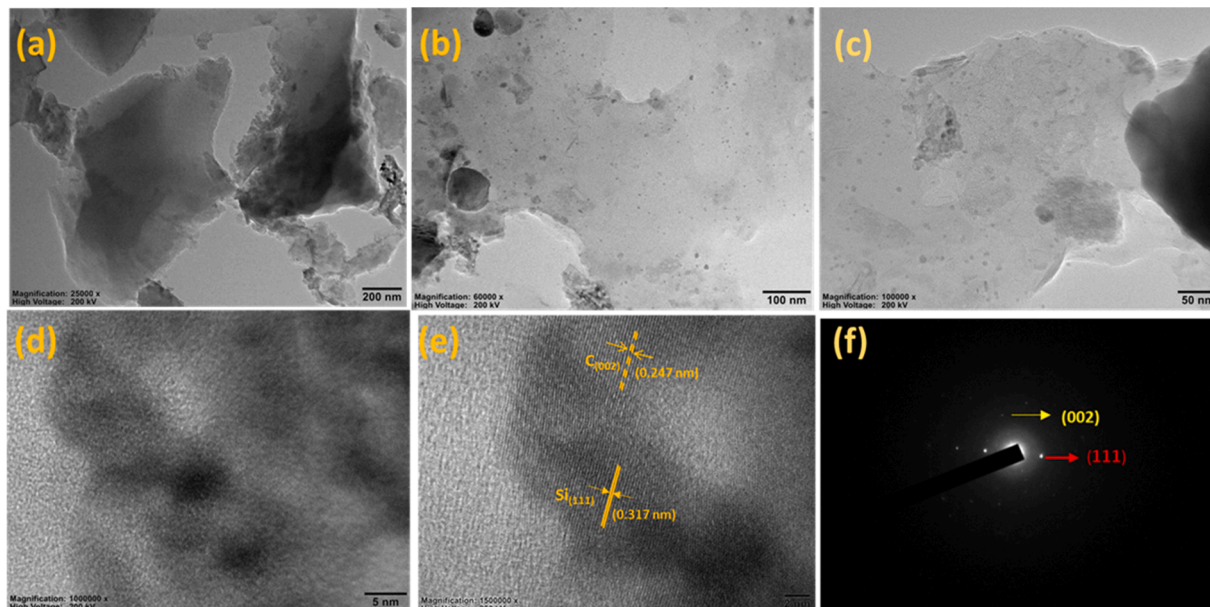
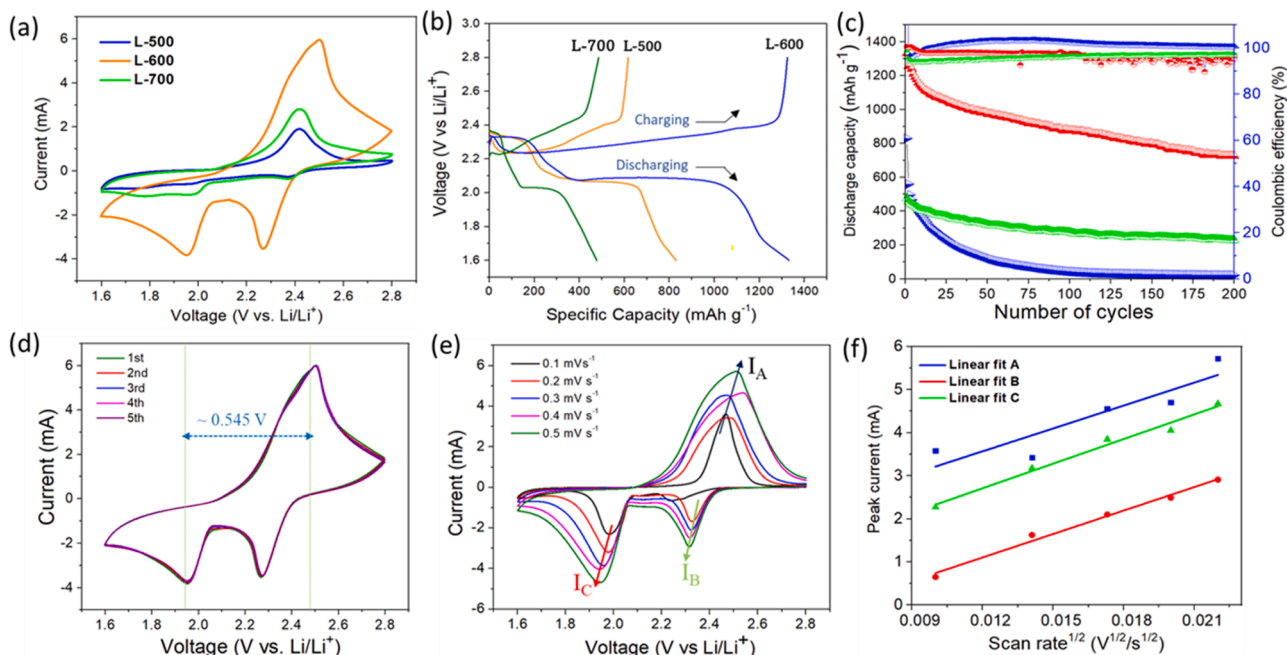


Fig. 4. (a-e) HR-TEM analysis of L-600 at different magnifications. (f) SAED pattern of L-600.



**Fig. 5.** (a) Comparative CV curve of L-X (L-500, L-600, and L-700) @  $0.5 \text{ mV s}^{-1}$ , (b) Comparative GCD of L-X @  $0.2 \text{ C}$  rate (1<sup>st</sup> cycle), (c) Cycling stability of L-X @  $0.2 \text{ C}$  for 200 cycles. CV curve of L-600 (d) @  $0.5 \text{ mV s}^{-1}$  for five cycles and (e) different scan rates, respectively. (f) Linear fit of CV peak currents vs scan rate of L-600.

l-600 effectively suppresses the diffusion of liquid intermediate products and loss of active materials, thus resulting in a high reversible specific capacity. To study the electrocatalytic activity of l-600, the diffusion rate of lithium-ion in Li-S battery with l-600 @ GF separator is measured by CV at different scan rates ranging from  $0.1$  to  $0.5 \text{ mV s}^{-1}$ , as shown in Fig. 5(e). The peak current  $I_A$ ,  $I_B$ , and  $I_C$  change with increased scan rates, and their peak potential changes more obviously. The diffusion coefficient of lithium-ion is calculated from the classical Randles-Sevcik equation [58]:

$$I_p = 2.69 \times 10^5 n^{3/2} A D_{Li}^{1/2} v^{1/2} C_{Li}$$

Here,  $I_p$  refers to the peak current,  $v$  corresponds to the scanning rate, and  $D_{Li}$  infers the diffusion coefficient of lithium ( $\text{Li}^+$ ) ions. According to the equation, the peak current  $I_p$  is directly proportional to the square root of both the scan rate ( $v$ ) and lithium ion diffusion coefficient ( $D_{Li}$ ). The higher  $I_p / v^{1/2}$  ratio implies the higher  $D_{Li}$  value, indicating more efficient and faster lithium ion diffusion. The linear analysis of  $D_{Li}$  for L-600 is shown in Fig. 5(f), and their values are found from their corresponding slopes as  $0.177$ ,  $0.181$ , and  $0.190$  for the peak A, B, and C, respectively. The slope values suggest a better ability of L-600 to promote the diffusion of lithium ions, which can promote the redox process

of lithium polysulfide to inhibit the shuttle effects.

The selective GCD profile of L-600 for 200 cycles @  $0.2 \text{ C}$  is shown in Fig. 6(a). This suggests that the cell with L-600-coated GF offers good stability even after 200 cycles, with a  $10\%$  capacity decrease from  $100$ – $200$  cycles. Two typical reduction plateaus centered at  $\sim 2.3$  and  $2.0 \text{ V}$  correspond to an intricate series of disproportionation conversion reactions, which is known to play a key role in the discharge-specific capacity, resulting in slow reaction kinetics [59]. For better capacitive performance, it is essential to have comparatively higher high-voltage plateau capacity ( $Q_H$ ) and low-voltage plateau capacity ( $Q_L$ ), indicating high sulfur utilization and enhanced conversion kinetics with lower polarization rate ( $\Delta E$ ), which specifies better redox reaction kinetics [60]. From Fig. 6(a), l-600 offers a higher  $Q_L$  than l-500 and l-700 and also a lower polarization rate ( $\Delta E$ ), which ensures enhanced conversion kinetics of polysulfides and better redox reaction kinetics [61]. The typical charge-discharge plateau of l-500 and l-700 for selective cycles from stability is compared in Figure S3 (a,b).

Furthermore, the porous carbon-coated separators assembled Li-S cells are subjected to electrochemical impedance spectroscopy analysis to verify the superiority of L-600 @ GF over the other L-X coated GF separators. The Nyquist plots obtained at an open circuit potential for L-500, L-600, and L-700 are shown in Fig. 6(b). All three cell's Nyquist

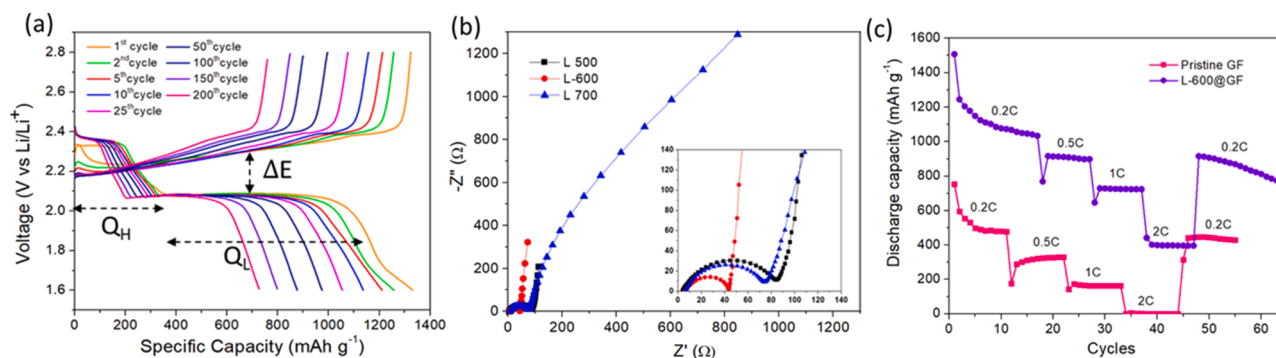


**Fig. 6.** (a) The selective GCD profile of L-600 for 200 cycles @  $0.2 \text{ C}$  rate. (b) EIS spectra of L-X (inset: high-frequency region) and (c) rate capability of pristine GF and L-600@GF separator at different C-rates.

plots exhibited a similar complete semicircle at the high-frequency region with an extended Warburg arm over the low-frequency region.  $R_s$  refers to the solution or ohmic resistance, depending on the electrode-electrolyte interface.  $R_{ct}$  corresponds to the charge transfer resistance, which is important in reflecting the reaction dynamics. The solution resistance ( $R_s$ ) was found to be 2.8, 4.6, 6.3  $\Omega$ , and its charge transfer resistance ( $R_{ct}$ ) was inferred as 85.2, 43.0, and 74.2  $\Omega$ , for L-500, L-600, and L-700, respectively. Comparatively, a lower  $R_{ct}$  and  $R_s$  value of L-600 agreed with better performance and significant specific capacity. In addition, the Warburg region over the low-frequency region is almost parallel to the imaginary impedance axis, indicating the high Li ion diffusion in the electrode-electrolyte interface [62]. The comparative Nyquist plot of Li-600@GF over pristine GF is shown in Figure S4. A rate capability study is carried out from 0.2C to 2C for L-600, as shown in Fig. 6(c), to investigate the capacity of Li-S cells to enable them in high-power applications. It is evident that the specific capacity steadily decreases with the increase in the current rate, ranging from 0.2 to 2 C. L-600 has a high initial discharge capacity of 1500  $\text{mAh g}^{-1}$  at the scan rate of 0.2 C, which is double times higher than that of pristine GF. Gradually, L-600 cells possess discharge-specific capacities of 1300, 918, 732, and 400  $\text{mAh g}^{-1}$  at 0.2C, 0.5C, 1C, and 2C, respectively. When the rate was returned to 0.2C, the discharge capacity was 924  $\text{mAh g}^{-1}$ , revealing the better reversibility of L-600. The enhanced electrochemical property of the L-600-coated separator over the pristine GF separator suggests the need for modification to reduce the polysulfide shuttling effect [63].

The polysulfide conversion process can be understood by analyzing the Galvanostatic Intermittent Titration Technique (GITT) response (Fig. 7 (a, d)) and reactive resistance trends during charge and discharge. The GITT was carried out at a 0.2 C current rate with a pulse of 10 min charge/discharge and 30 min rest. The obtained GITT for the L-600 modified separator in the Li-S battery is shown in Fig. 7(a). The voltage response during intermittent titration exhibits distinct plateaus

corresponding to the multi-step conversion of sulfur species ( $\text{S}_8 \rightarrow \text{Li}_2\text{S}_6 \rightarrow \text{Li}_2\text{S}_4 \rightarrow \text{Li}_2\text{S}_2 \rightarrow \text{Li}_2\text{S}$ ) [64]. The sharp voltage drops and subsequent recovery in the discharge phase are associated with  $\text{Li}_2\text{S}$  nucleation and activation. Lithium polysulfides gradually convert into a highly insulating solid  $\text{Li}_2\text{S}$  phase at a lower voltage, increasing the overpotential. During charging,  $\text{Li}_2\text{S}$  activation occurs, but the slow dissolution kinetics cause a gradual increase in internal resistance. The Li-S cell with the modified separator delivers a discharge capacity of 825  $\text{mAh g}^{-1}$  at 0.2 C (Fig. 7(b)), indicating efficient sulfur utilization. The state of charge (SOC) and state of discharge (SOD) were calculated based on the delivered capacity relative to the theoretical capacity of sulfur (1675  $\text{mAh g}^{-1}$ ). During charging (Fig. 7(c)), the reactive resistance decreases continuously upto 700  $\text{mAh g}^{-1}$  (SOC = 0.418) before increasing. This suggests that in the early stages of charging, lower-order polysulfides ( $\text{Li}_2\text{S}_2/\text{Li}_2\text{S}$ ) dissolve into higher-order polysulfides ( $\text{Li}_2\text{S}_6$ ,  $\text{Li}_2\text{S}_8$ ), reducing resistance. However, beyond SOC = 0.418, the increase in resistance indicates that sulfur is being redeposited as a solid, slowing charge transfer kinetics. During discharge (Figure 7(c)), the reactive resistance remains stable at 0.8  $\Omega \text{ g}$  up to 357  $\text{mAh g}^{-1}$  (SOD = 0.213), suggesting a smooth conversion of sulfur ( $\text{S}_8$ ) into higher-order polysulfides ( $\text{Li}_2\text{S}_8$ ,  $\text{Li}_2\text{S}_6$ ). Beyond this point, resistance increases significantly, reaching 4.9  $\Omega \text{ g}$  at SOD = 0.423, which correlates with the formation of low-order polysulfides ( $\text{Li}_2\text{S}_2/\text{Li}_2\text{S}$ ) [65]. These species are less soluble and begin precipitating on the cathode, increasing polarization and reducing the electrochemical kinetics. The overall discharge process follows a stepwise reduction of sulfur into polysulfides, initially forming soluble  $\text{Li}_2\text{S}_8$  and  $\text{Li}_2\text{S}_6$ , which then converted into insoluble  $\text{Li}_2\text{S}_2$  and  $\text{Li}_2\text{S}$ , causing an increase in resistance [66]. Conversely, solid  $\text{Li}_2\text{S}$  is reoxidized to soluble polysulfides during charging, reducing resistance up to SOC = 0.418, after which sulfur deposition increases resistance. The observed resistance trends confirm the sequential polysulfide conversion during charge and discharge, highlighting the role of the modified separator in maintaining lower resistance during early

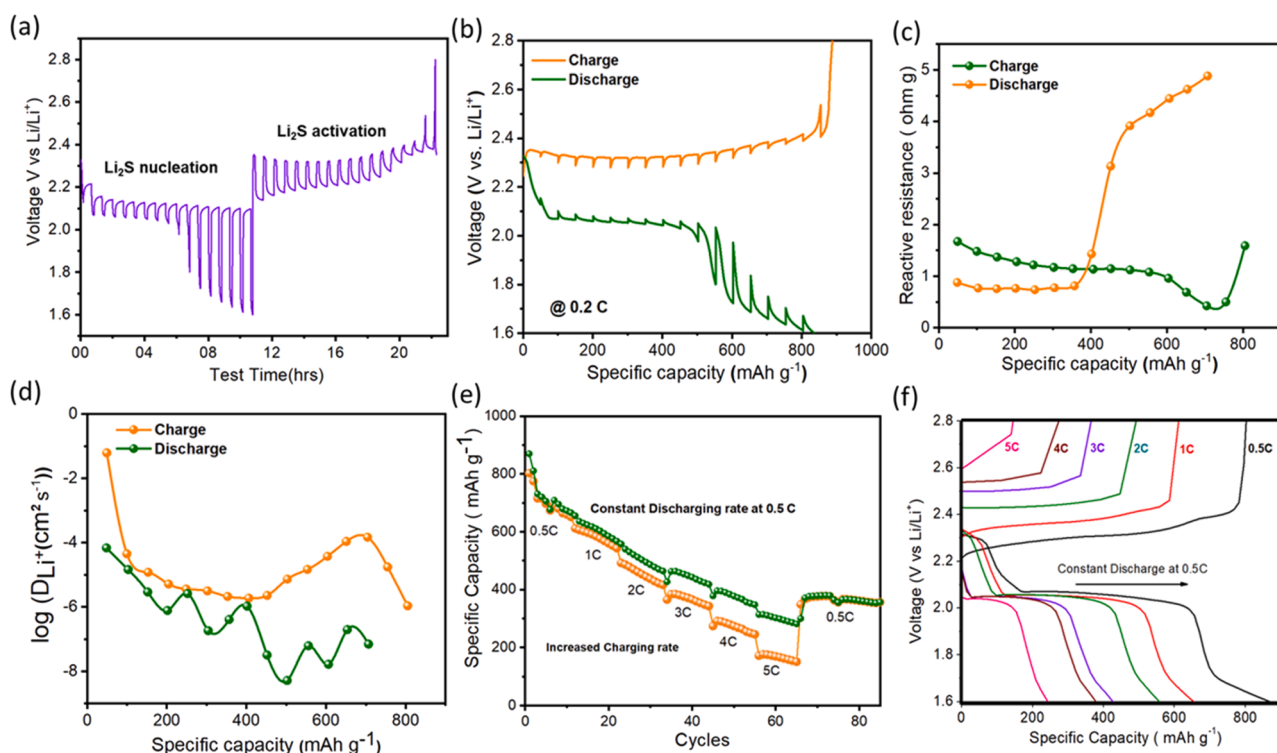


**Fig. 7.** (a) GITT profile of L-600, the cell was allowed to relax for 30 min after every 10 min charge/discharge at @ 0.2 C rate. (b) GITT potential response as a function of specific capacity. (c) Comparative reactive resistance trend and (d) diffusion coefficient variation with specific capacity during charge and discharge. (e) Rate capability comparison of L-600@ GF separator for fast charging analysis at various charging rates (0.5 C to 5 C) with constant discharge at 0.5 C and (f) corresponding GCD profile.



discharge. The rise in resistance beyond specific SOC and SOD values indicates  $\text{Li}_2\text{S}$  precipitation during discharge and sulfur deposition during charging. A similar observation is also noticed in the  $\text{SnS}$ /porous carbon nanosheet-modified Celgard separator for Li-S batteries [58]. The average reactive resistance for the charging and discharging process is 1.12-ohm g and 2.27-ohm g. Fig. 7(d) presents the lithium-ion diffusion coefficients of the L-600 modified separator. The diffusion coefficient trend during the whole discharge and charge process of the cell was calculated using Fick's second law of diffusion, given below

$$D_{\text{Li}^+} = \frac{4}{\pi\tau} \left( \frac{m_B V_m}{M_B S} \right)^2 \left( \frac{\Delta E_s}{\Delta E_t} \right)^2$$

Here,  $\tau$  is the time duration for the current pulse,  $m_B$  represents the active mass of the electrode,  $M_B$  is the molar mass of the active material, and  $S$  corresponds to the area of the electrode in contact with the electrolyte.  $V_m$  symbolizes the molar volume of the sulfur cathode.  $\Delta E_s$  and  $\Delta E_t$  are the changes in the constant current pulse and equilibrium potential. Fig. 7(d) presents the values of diffusion acquired during the charge and discharge of different potentials. The average diffusion

coefficient during the charging and discharging process is  $3.68 \times 10^{-4} \text{ cm}^2 \text{ s}^{-1}$  and  $6.48 \times 10^{-6} \text{ cm}^2 \text{ s}^{-1}$ . During charging, lithium sulfide ( $\text{Li}_2\text{S}$ ) is converted back into soluble higher-order polysulfides ( $\text{Li}_2\text{S}_6$ ,  $\text{Li}_2\text{S}_8$ ), which are more mobile, resulting in a higher diffusion coefficient. In contrast, during discharging, the formation of insoluble  $\text{Li}_2\text{S}_2/\text{Li}_2\text{S}$  near the cathode restricts ion transport, leading to a lower diffusion coefficient.

Practically, the critical challenge for enabling Li-S batteries in electric vehicles targets its fast-charging ability. Charging time can be reduced by increasing the charging current, but it may simultaneously accelerate battery degradation. Therefore, the charging rate has a more significant effect on battery degradation than the discharge rate [67]. The optimized Li-S cell with L-600 modified separator is subjected to fast charging studies, and Fig. 7(e) shows the charge-discharge profile with various charging rates as 0.5C, 1C, 2C, 3C, 4C, and 5C with constant discharging at 0.5C. Fig. 7(f) shows the corresponding fast-charging specific capacity retention rate, which depicts better recyclability even when the charging rate (5C) is increased 10 times more than the discharging rate (0.5C). The enhanced Li-S battery performance of L-600

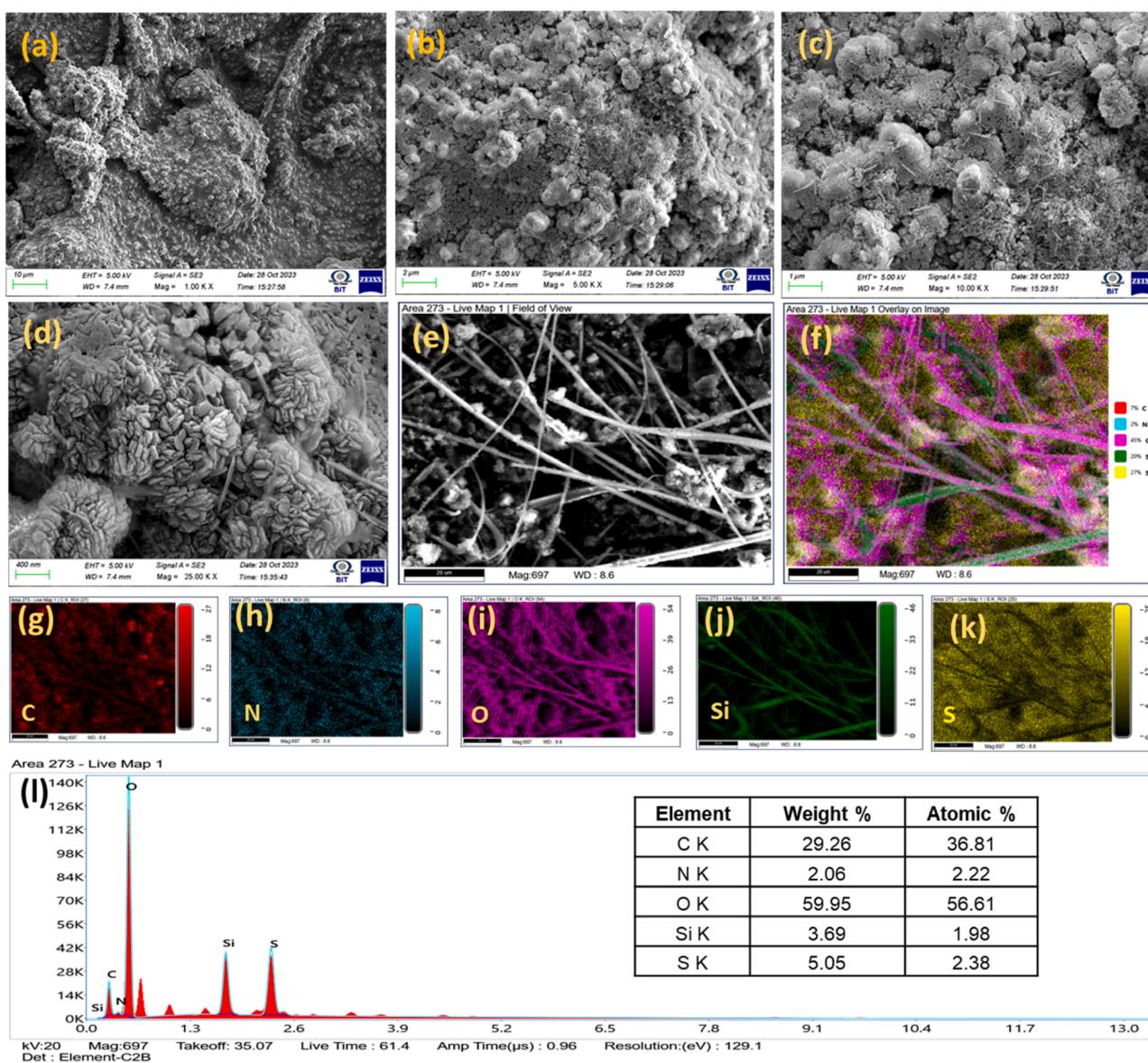


**Fig. 8.** (a-d) FESEM images of l-600@GF separator after stability at different magnifications. (e) Selected complete area for elemental mapping. (f) combined elemental mapping along with (g) carbon (C), (h) nitrogen (N), (i) oxygen (O), (j) silicon (Si), and (k) sulfur (S) respectively. (l) FESEM-EDS spectrum (inset: elemental distribution ratio).

coated GF over the L-500, L-700, and Pristine GF is credited to the uniform, unique 3D porous structure with complex functional groups associated with the carbon matrix, as discussed. The performance matrix of the L-600 modified separator for Li-S battery in terms of initial capacity and capacity retention is compared with the recent literature and given in Table S2. Therefore, it is evident that the L-600 modified separator offers high specific capacity and capacitance retention, thereby promising to suppress the polysulfide shuttling and dendrite formation in the anode.

### 3.3. Post-Mortem study

Postmortem analyses were carried out to analyze the polysulfide shuttling effect of the L-600 modified separator after cycling. After 200 cycles, the dismantled separator was subjected to FESEM analysis, and its surface morphology at different magnifications is shown in Fig. 8 (a-d), respectively. The deposited materials over the porous carbon region coated on the GF separator suggest a strong matrix to absorb, seize, and hold the polysulfides owing to electrochemical deposition at the end of charge/ discharge reactions [68]. An EDX inspection after cycling stability exhibited elemental C, N, O, Si, and S on the separator, which is uniformly deposited over the L-600 modified separator matrix, as shown in Fig. 8 (e-k), respectively. This deposition over the GF-modified L-600, which faced the cathode, clearly exhibits absorption and interception properties of the porous carbon coating. Additionally, the sulfur signals in the corresponding EDX spectrum (Fig. 8(l)) show active sulfur materials uniformly embedded over the carbon, providing that the porous regime effectively traps the soluble polysulfides and retains them as active material on the cathode side [69].

## 4. Conclusion

The physicochemical analysis states the uniqueness of lichen-derived carbon material attributed to naturally embedded silicon functional groups and a well-defined porous network that can play a vital role in polysulfide shuttling. In addition, the calcination temperature of lichen biomass was also optimized and found to be L-600, which offers graphitic nanostructures along with the complex functional groups observed through Raman, FTIR, and XPS analysis, respectively. Interestingly, the electrochemical performance of L-600 was consistent with the physicochemical analysis, with a high specific capacity of 1330 mAh g<sup>-1</sup> at 0.2 C and a high reversible capacity of 725 mAh g<sup>-1</sup> after 200 cycles, with a degradation rate of 0.22 % per cycle. Notably, the significant performance is attributed to the diverse functional groups and three-dimensional porous networks associated with L-600 observed through BET and FESEM analysis. As a result, the Li-S cell mounted with a modified GF separator offers less R<sub>s</sub> and R<sub>ct</sub> values with ideal battery performance. This remarkable performance is attributed to lichen in situ in the lichen biomass. The interconnected foam-like porous network and better graphitization in L-600 facilitated efficient electron/ion transport and effectively trapped lithium polysulfides, reducing the shuttle effect and enhancing cycling stability. Therefore, this work proposed an effective and eco-friendly method of modifying GF separators for future Li-S batteries with promising energy storage applications.

### CRedit authorship contribution statement

**Krishnan Vignesh:** Writing – original draft, Methodology, Investigation, Formal analysis, Data curation. **Tamilarasan Mathivanan:** Methodology, Data curation. **Mariappan Ganeshbabu:** Methodology, Formal analysis, Data curation. **Nuthalapati Prasanna Naga Puneeth:** Methodology, Investigation, Data curation. **Balasubramaniam Ramakumar:** Resources. **Yun Sung Lee:** Resources. **Ramakrishnan Kalai Selvan:** Writing – review & editing, Writing – original draft, Supervision, Resources, Project administration, Methodology, Formal analysis, Conceptualization.

## Declaration of competing interest

The authors declare that they have no known competing financial interests or personal relationships that could have appeared to influence the work reported in this paper.

## Acknowledgment

Dr. RKS gratefully acknowledges SERB (CRG/2018/001995 dated 09.04.2019) for the financial support and the DST-FIST program for establishing the Glovebox facility. The authors also acknowledge the HRTEM facility, Central Instrumentation Center (CIC), Bharathiar University, supported by the DST-PURSE Phase-II program. Prof. Yun-Sung Lee acknowledges the financial support from the National Research Foundation of Korea (NRF) grant funded by the Korean government (Ministry of Science, ICT & Future Planning) (No. RS-2023-00208361).

## Supplementary materials

Supplementary material associated with this article can be found, in the online version, at [doi:10.1016/j.cartre.2025.100545](https://doi.org/10.1016/j.cartre.2025.100545).

## Data availability

Data will be made available on request.

## References

- [1] C. Li, R. Liu, Y. Xiao, F. Cao, H. Zhang, Recent progress of separators in lithium-sulfur batteries, *Energy Storage Mater* 40 (2021) 439–460, <https://doi.org/10.1016/j.ensm.2021.05.034>.
- [2] W. Ren, W. Ma, S. Zhang, B. Tang, Recent advances in shuttle effect inhibition for lithium sulfur batteries, *Energy Storage Mater* 23 (2019) 707–732, <https://doi.org/10.1016/j.ensm.2019.02.022>.
- [3] Z. Wang, Y. Li, H. Ji, J. Zhou, T. Qian, C. Yan, Unity of opposites between soluble and insoluble lithium polysulfides in lithium–Sulfur batteries, *Adv. Mater.* 34 (2022) 2203699, <https://doi.org/10.1002/adma.202203699>.
- [4] A. Manthiram, A reflection on lithium-ion battery cathode chemistry, *Nat. Commun.* 11 (2020) 1550, <https://doi.org/10.1038/s41467-020-15355-0>.
- [5] N. Nitta, F. Wu, J.T. Lee, G. Yushin, Li-ion battery materials: present and future, *Mater. Today* 18 (2015) 252–264, <https://doi.org/10.1016/j.matod.2014.10.040>.
- [6] S. Mahmud, M. Rahman, M. Kamruzzaman, M.O. Ali, M.S.A. Emon, H. Khatun, M. R. Ali, Recent advances in lithium-ion battery materials for improved electrochemical performance: a review, *Results Eng* 15 (2022) 100472, <https://doi.org/10.1016/j.rineng.2022.100472>.
- [7] N. Nakamura, S. Ahn, T. Momma, T. Osaka, Future potential for lithium-sulfur batteries, *J. Power Sources* 558 (2023) 232566, <https://doi.org/10.1016/j.jpowsour.2022.232566>.
- [8] Z. Wang, Z. Du, L. Wang, G. He, I.P. Parkin, Y. Zhang, Y. Yue, Disordered materials for high-performance lithium-ion batteries: a review, *Nano Energy* 121 (2024) 109250, <https://doi.org/10.1016/j.nanoen.2023.109250>.
- [9] Y. Jiang, Y. Liao, J. Yu, X. Li, T. Jin, Y. Xu, W. Li, S. Huang, S. Xia, B. Zhao, X. Sun, J. Zhang, Multi-effect ionic liquid additives achieve high cycle stability lithium-sulfur batteries by constructing an electrostatic shielding layer and eliminating ‘dead sulfur’, *Adv. Funct. Mater.* (2025) 2500077, <https://doi.org/10.1002/adfm.202500077>.
- [10] J. Li, L. Sun, G. Lv, L. Liao, Application of clay minerals in lithium-sulfur batteries: a review, *J. Energy Storage* 106 (2025) 114852, <https://doi.org/10.1016/j.est.2024.114852>.
- [11] J.M. Gonçalves, É.A. Santos, P.R. Martins, C.G. Silva, H. Zanin, Emerging medium- and high-entropy materials as catalysts for lithium-sulfur batteries, *Energy Storage Mater* 63 (2023) 102999, <https://doi.org/10.1016/j.ensm.2023.102999>.
- [12] J.-L. Popien, C. Thies, A. Barke, T.S. Spengler, Comparative sustainability assessment of lithium-ion, lithium-sulfur, and all-solid-state traction batteries, *Int. J. Life Cycle Assess.* 28 (2023) 462–477, <https://doi.org/10.1007/s11367-023-02134-4>.
- [13] Y. Shi, G. Xu, G. Liang, D. Lan, S. Zhang, Y. Wang, D. Li, G. Wu, PEG-VN modified PP separator for high-stability and high-efficiency lithium-sulfur batteries, *Acta Physico-Chimica Sin* 41 (2025) 100082, <https://doi.org/10.1016/j.actphy.2025.100082>.
- [14] L. Yu, J. Gu, C. Pan, J. Zhang, Z. Wei, Y. Zhao, Recent developments of composite separators based on high-performance fibers for lithium batteries, *Compos. Part A Appl. Sci. Manuf.* 162 (2022) 107132, <https://doi.org/10.1016/j.compositesa.2022.107132>.
- [15] L. Zhan, X. Zhou, J. Luo, X. Fan, X. Ning, Urchin-like Nb<sub>2</sub>O<sub>5</sub>/CNT modified separator for lithium-sulfur batteries, *Int. J. Hydrogen Energy* 47 (2022) 27671–27679, <https://doi.org/10.1016/j.ijhydene.2022.06.089>.



- [16] Y. Wang, B. Yue, X. Yan, Y. Fang, J. Wang, Q. Ma, G. Liu, W. Yu, X. Dong, Tailored PPy-coated CeO<sub>2</sub>/Co<sub>3</sub>O<sub>4</sub> yolk-shell nanostructures: engineering sulfur hosts for high-performance lithium-sulfur batteries, *Chem. Eng., J.* 518 (2025) 164649, <https://doi.org/10.1016/j.cej.2025.164649>.
- [17] Y.-C. Lin, Y.-H. Wu, J.-M. Ting, S.-H. Chung, Stable lithium-Sulfur cell separator with a high-entropy metal oxide modification, *Energy Fuels* 37 (2023) 15162–15169, <https://doi.org/10.1021/acs.energyfuels.3c02538>.
- [18] H. Zhang, R. Dai, S. Zhu, L. Zhou, Q. Xu, Y. Min, Bimetallic nitride modified separator constructs internal electric field for high-performance lithium-sulfur battery, *Chem. Eng. J.* 429 (2022) 132454, <https://doi.org/10.1016/j.cej.2021.132454>.
- [19] K. Zhang, F. Zhang, H. Pan, J. Yu, L. Wang, D. Wang, L. Wang, G. Hu, J. Zhang, Y. Qian, Dual taming of polysulfides by phosphorus-doped carbon for improving electrochemical performances of lithium-sulfur battery, *Electrochim. Acta* 354 (2020) 136648, <https://doi.org/10.1016/j.electacta.2020.136648>.
- [20] P. Li, H. Lv, Z. Li, X. Meng, Z. Lin, R. Wang, X. Li, The electrostatic attraction and catalytic effect enabled by ionic-Covalent organic nanosheets on MXene for separator modification of lithium-Sulfur batteries, *Adv. Mater.* 33 (2021) 202007803, <https://doi.org/10.1002/adma.202007803>.
- [21] S. Jiang, M. Chen, X. Wang, Y. Zhang, C. Huang, Y. Zhang, Y. Wang, Honeycomb-like nitrogen and sulfur dual-doped hierarchical porous biomass carbon bifunctional interlayer for advanced lithium-sulfur batteries, *Chem. Eng. J.* 355 (2019) 478–486, <https://doi.org/10.1016/j.cej.2018.08.170>.
- [22] L. Zhu, L. You, P. Zhu, X. Shen, L. Yang, K. Xiao, High performance lithium-Sulfur batteries with a sustainable and environmentally friendly carbon aerogel modified separator, *ACS Sustain. Chem. Eng.* 6 (2018) 248–257, <https://doi.org/10.1021/acssuschemeng.7b02322>.
- [23] Fan Wang, H. Yuan, J. Huang, A bio-inspired nanofibrous Co<sub>3</sub>O<sub>4</sub>/TiO<sub>2</sub>/carbon composite as high-performance anodic material for lithium-ion batteries, *J. Alloys Compd.* 819 (2020) 153375, <https://doi.org/10.1016/j.jallcom.2019.153375>.
- [24] J. Li, J. Yu, Y. Zhang, C. Li, Y. Ma, H. Ge, N. Jian, L. Li, C.Y. Zhang, J.Y. Zhou, J. Arbiol, A. Cabot, Boosting polysulfide conversion on Fe-doped nickel diselenide toward robust lithium-Sulfur batteries, *Adv. Funct. Mater.* (2025) 2501485, <https://doi.org/10.1002/adfm.202501485>.
- [25] Y. Zhao, X. Zhang, Y. He, N. Liu, T. Tan, C. Liang, Biomass derived nitrogen-doped highly porous carbon material with a hierarchical porous structure for high-performance lithium/sulfur batteries, *Materials (Basel)* 10 (2017) 1158, <https://doi.org/10.3390/ma10101158>.
- [26] H. Zhu, X. He, Z. Xu, L. Dai, Deep eutectic solvent-mediated hydrothermal treatment for biomass conversion: a review, *Green Chem.* 27 (2024) 1278–1299, <https://doi.org/10.1039/d4gc05662k>.
- [27] Q. Li, Y. Liu, L. Yang, Y. Wang, Y. Liu, Y. Chen, X. Guo, Z. Wu, B. Zhong, N. O co-doped chlorella-based biomass carbon modified separator for lithium-sulfur battery with high capacity and long cycle performance, *J. Colloid Interface Sci.* 585 (2021) 43–50, <https://doi.org/10.1016/j.jcis.2020.11.084>.
- [28] H. Parsimehr, A. Ehsani, Algae-based electrochemical energy storage devices, *Green Chem* 22 (2020) 8062–8096, <https://doi.org/10.1039/D0GC02246B>.
- [29] Y. Xia, R. Fang, Z. Xiao, H. Huang, Y. Gan, R. Yan, X. Lu, C. Liang, J. Zhang, X. Tao, W. Zhang, Confining sulfur in N-doped porous carbon microspheres derived from microalgae for advanced lithium-Sulfur batteries, *ACS Appl. Mater. Interfaces* 9 (2017) 23782–23791, <https://doi.org/10.1021/acsami.7b05798>.
- [30] D. Zalka, A. Vizintin, A. Maximenko, Z. Pászti, Z. Dankházi, K. Hegedüs, L. S. Shankar, R. Kun, K. Saksal, A.S. Fedoroková, P. Jován, Improving lithium-sulfur battery performance using a polysaccharide binder derived from red algae, *Commun. Mater.* 6 (2025) 17, <https://doi.org/10.1038/s43246-025-00734-1>.
- [31] D.S. Priya, L.J. Kennedy, G.T. Anand, Emerging trends in biomass-derived porous carbon materials for energy storage application: a critical review, *Mater. Today Sustain.* 21 (2023) 100320, <https://doi.org/10.1016/j.mtsust.2023.100320>.
- [32] L. Furmanek, P. Czarnota, M.R.D. Seaward, A review of the potential of lichen substances as antifungal agents: the effects of extracts and lichen secondary metabolites on fusarium fungi, *Arch. Microbiol.* 204 (2022) 523, <https://doi.org/10.1007/s00203-022-03104-4>.
- [33] J. Igoli, A. Gray, C. Clements, P. Kantheti, R. Singla, Antitrypanosomal activity & docking studies of isolated constituents from the Lichen *Cetraria islandica*: possibly multifunctional scaffolds, *Curr. Top. Med. Chem.* 14 (2014) 1014–1021, <https://doi.org/10.2174/1568026614666140324122323>.
- [34] R. Kalai Selvan, P. Zhu, C. Yan, J. Zhu, M. Dirican, A. Shanmugavani, Y.S. Lee, X. Zhang, Biomass-derived porous carbon modified glass fiber separator as polysulfide reservoir for Li-S batteries, *J. Colloid Interface Sci.* 513 (2018) 231–239, <https://doi.org/10.1016/j.jcis.2017.11.016>.
- [35] B. Liu, X. Wu, S. Wang, Z. Tang, Q. Yang, G.-H. Hu, C. Xiong, Flexible carbon nanotube modified separator for high-performance lithium-sulfur batteries, *Nanomaterials* 7 (2017) 196, <https://doi.org/10.3390/nano7080196>.
- [36] H. Duan, H. Xu, Q. Wu, L. Zhu, Y. Zhang, B. Yin, H. He, Silicon/graphite/amorphous carbon as anode materials for lithium secondary batteries, *Molecules* 28 (2023) 464, <https://doi.org/10.3390/molecules28020464>.
- [37] M. Cabello, E. Gucciardi, A. Herrán, D. Carriazo, A. Villaverde, T. Rojo, Towards a high-power Si@graphite anode for lithium ion batteries through a wet ball milling process, *Molecules* 25 (2020) 2494, <https://doi.org/10.3390/molecules25112494>.
- [38] T.L. de Vasconcelos, A.K. de Oliveira, E.C. Pereira, N.H. da Silva, C. Vicente, M.-E. Legaz, The lichen *Cladonia verticillaris* retains and modifies mineral soil particles inside the thallus, *CATENA* 135 (2015) 70–77, <https://doi.org/10.1016/j.catena.2015.07.002>.
- [39] N. Prasanna Naga Puneeth, K. Rajkumar, A. Soundarya, S.D. Kaushik, Y.S. Lee, S. Park, R. Kalai Selvan, Nano-graphitic crystallites effect on the improved K-ion intercalation properties of *Kigelia Africana* fruit-derived hard carbon for potassium-ion batteries, *Chem. Eng. J.* 480 (2024) 147835, <https://doi.org/10.1016/j.cej.2023.147835>.
- [40] S. Yu, H. Wang, C. Hu, Q. Zhu, N. Qiao, B. Xu, Facile synthesis of nitrogen-doped, hierarchical porous carbons with a high surface area: the activation effect of a nano-ZnO template, *J. Mater. Chem. A* 4 (2016) 16341–16348, <https://doi.org/10.1039/C6TA07047G>.
- [41] S. Muthomimah, W. Rahayu, A. Aliyatulmuna Nazriati, Effect of sonication frequency in synthesis of silica aerogel-activated carbon nanocomposite, *IOP Conf. Ser. Mater. Sci. Eng.* 833 (2020) 012077, <https://doi.org/10.1088/1757-899X/833/1/012077>.
- [42] K. Rajkumar, M. Ragupathi, Y. Sung Lee, R. Kalai Selvan, Preparation of sponge-like porous carbon from *Ficus Religiosa* leaf and its K-ion intercalation properties, *Mater. Lett.* 301 (2021) 130298, <https://doi.org/10.1016/j.matlet.2021.130298>.
- [43] L. Zhu, H. Jiang, Q. Yang, S. Yao, X. Shen, F. Tu, An effective porous activated carbon derived from puffed corn employed as the separator coating in a lithium-Sulfur battery, *Energy Technol* 7 (2019) 1900752, <https://doi.org/10.1002/ente.201900752>.
- [44] S. Shanmugapriya, P. Zhu, M. Ganeshbabu, Y. Sung Lee, X. Zhang, R. Kalai Selvan, Improved electrocatalytic properties of bundled B/N co-doped electrospun carbon nanofibers with Pt nanostructures through dopant-induced metal-support interaction (DIMSI), *Mater. Sci. Eng. B* 284 (2022) 115880, <https://doi.org/10.1016/j.mseb.2022.115880>.
- [45] T. Yang, X. Tian, Y. Song, S. Wu, J. Wu, Z. Liu, Oxygen-doped carbon nanofiber nonwovens as an effective interlayer towards accelerating electrochemical kinetics for lithium-sulfur battery, *Appl. Surf. Sci.* 611 (2023) 155690, <https://doi.org/10.1016/j.apsusc.2022.155690>.
- [46] K. Xiang, S. Cai, X. Wang, M. Chen, S. Jiang, Nitrogen-doped activated microporous carbon spheres as a sulfur matrix for advanced lithium-sulfur batteries, *J. Alloys Compd.* 740 (2018) 687–694, <https://doi.org/10.1016/j.jallcom.2018.01.026>.
- [47] P. Zeng, L. Huang, X. Zhang, R. Zhang, L. Wu, Y. Chen, Long-life and high-areal-capacity lithium-sulfur batteries realized by a honeycomb-like N, P dual-doped carbon modified separator, *Chem. Eng. J.* 349 (2018) 327–337, <https://doi.org/10.1016/j.cej.2018.05.096>.
- [48] A. Kim, S.H. Oh, A. Adhikari, B.R. Sathe, S. Kumar, R. Patel, Recent advances in modified commercial separators for lithium-sulfur batteries, *J. Mater. Chem. A* 11 (2023) 7833–7866, <https://doi.org/10.1039/D2TA09266B>.
- [49] M. Vijayakumar, N. Govind, E. Walter, S.D. Burton, A. Shukla, A. Devaraj, J. Xiao, J. Liu, C. Wang, A. Karim, S. Thevuthasan, Molecular structure and stability of dissolved lithium polysulfide species, *Phys. Chem. Chem. Phys.* 16 (2014) 10923–10932, <https://doi.org/10.1039/C4CP00889H>.
- [50] G. Li, J. Sun, W. Hou, S. Jiang, Y. Huang, J. Geng, Three-dimensional porous carbon composites containing high sulfur nanoparticle content for high-performance lithium-sulfur batteries, *Nat. Commun.* 7 (2016) 10601, <https://doi.org/10.1038/ncomms10601>.
- [51] W. Huang, D. Ruan, H. Chen, K. Hu, J. Wen, W. Yan, Y. Zhu, Y. Zhang, N. Yu, Y. Wu, A three-dimensional interconnected nitrogen-doped graphene-like porous carbon-modified separator for high-performance Li-S batteries, *Sustain. Energy Fuels* 4 (2020) 4264–4272, <https://doi.org/10.1039/D0SE00620C>.
- [52] R. Li, Z. Shen, H. Zheng, L. Jin, Y. Zhang, W. Yuan, X. Wang, Three-dimensional nitrogen and oxygen co-doped hierarchical porous carbons prepared from polyacrylonitrile/polyamic acid composite films for supercapacitors, *J. Energy Storage* 73 (2023) 109521, <https://doi.org/10.1016/j.est.2023.109521>.
- [53] A. Raulo, A. Gupta, R. Srivastava, B. Nandan, Excellent electrochemical performance of lithium-sulfur batteries via self-standing cathode from interwoven α-Fe<sub>2</sub>O<sub>3</sub> integrated carbon nanofiber networks, *J. Electroanal. Chem.* 880 (2021) 114829, <https://doi.org/10.1016/j.jelechem.2020.114829>.
- [54] T. Mathivanan, N. Panjulingam, S. Dolui, S. Lakshminpathi, S. Banerjee, R. Kalai Selvan, Enhancement of electrochemical performances of Li-S batteries using PPESK and Nelumbo nucifera derived porous carbon modified separator, *Mater. Lett.* 315 (2022) 131935, <https://doi.org/10.1016/j.matlet.2022.131935>.
- [55] W. Bao, D. Su, W. Zhang, X. Guo, G. Wang, 3D Metal carbide/mesoporous carbon hybrid architecture as a new polysulfide reservoir for lithium-sulfur batteries, *Adv. Funct. Mater.* 26 (2016) 8746–8756, <https://doi.org/10.1002/adfm.201603704>.
- [56] N.K. Thangavel, D. Gopalakrishnan, L.M.R. Arava, Understanding heterogeneous electrocatalysis of lithium polysulfide redox on Pt and WS<sub>2</sub> surfaces, *J. Phys. Chem. C* 121 (2017) 12718–12725, <https://doi.org/10.1021/acs.jpcc.7b01514>.
- [57] C. Xian, P. Jing, X. Pu, G. Wang, Q. Wang, H. Wu, Y. Zhang, A trifunctional separator based on a blockage-adsorption-catalysis synergistic effect for Li-S batteries, *ACS Appl. Mater. Interfaces* 12 (2020) 47599–47611, <https://doi.org/10.1021/acsami.0c14645>.
- [58] Z. Li, F. Zhang, T. Cao, L. Tang, Q. Xu, H. Liu, Y. Wang, Highly stable lithium-Sulfur batteries achieved by a SnS/porous carbon nanosheet architecture modified celgard separator, *Adv. Funct. Mater.* 30 (2020) 2006297, <https://doi.org/10.1002/adfm.202006297>.
- [59] T. Mathivanan, S. Dolui, P. Nandhini, K. Rajkumar, S. Lakshminpathi, S. Banerjee, R. Kalai Selvan, Experimental and theoretical analysis of synthesized poly (Phthalazine Ether Sulfone Ketone) copolymer-modified separators for Li-S batteries, *ChemElectroChem* 9 (2022) e202200561, <https://doi.org/10.1002/celec.202200561>.
- [60] H. Watanabe, Y. Sugiura, S. Seki, J. Han, I. Shitanda, M. Itagaki, Y. Umebayashi, Discharge behavior within lithium-Sulfur batteries using Li-Glyme solvate ionic liquids, *J. Phys. Chem. C* 127 (2023) 6645–6654, <https://doi.org/10.1021/acs.jpcc.3c00447>.
- [61] X. Yang, R. Li, J. Yang, H. Liu, T. Luo, X. Wang, L. Yang, A novel route to constructing high-efficiency lithium sulfur batteries with spent graphite as the



- sulfur host, Carbon N. Y. 199 (2022) 215–223, <https://doi.org/10.1016/j.carbon.2022.06.067>.
- [62] A. Shodiev, E.N. Primo, M. Chouchane, T. Lombardo, A.C. Ngandjong, A. Rucci, A. A. Franco, 4D-resolved physical model for Electrochemical impedance spectroscopy of  $\text{Li}(\text{Ni}_{1-x-y}\text{Mn}_x\text{Co}_y)\text{O}_2$ -based cathodes in symmetric cells: consequences in tortuosity calculations, J. Power Sources 454 (2020) 227871, <https://doi.org/10.1016/j.jpowsour.2020.227871>.
- [63] C. Dong, C. Zhou, M. Wu, Y. Yu, K. Yu, K. Yan, C. Shen, J. Gu, M. Yan, C. Sun, L. Mai, X. Xu, Boosting Bi-directional redox of sulfur with dual metal single atom pairs in carbon spheres toward high-rate and long-cycling lithium–Sulfur battery, Adv. Energy Mater. 13 (2023) 2301505, <https://doi.org/10.1002/aenm.202301505>.
- [64] F.L. Lama, V. Marangon, Á. Caballero, J. Morales, J. Hassoun, Diffusional features of a lithium-sulfur battery exploiting highly microporous activated carbon, ChemSusChem 16 (2023) e202202095, <https://doi.org/10.1002/cssc.202202095>.
- [65] Z. Liu, C. Lu, S. Yuan, X. Ren, Y. Chen, Nickel-embedded hierarchically-porous carbon microspheres as a multifunctional separator modifier for achieving advanced lithium-sulfur batteries, J. Alloys Compd. 960 (2023) 170844, <https://doi.org/10.1016/j.jallcom.2023.170844>.
- [66] B. Wang, L. Wang, B. Zhang, S. Zeng, F. Tian, J. Dou, Y. Qian, L. Xu, Niobium diboride nanoparticles accelerating polysulfide conversion and directing Li 2 S nucleation enabled high areal capacity lithium–Sulfur batteries, ACS Nano 16 (2022) 4947–4960, <https://doi.org/10.1021/acsnano.2c01179>.
- [67] H. Kang, H. Kim, M.J. Park, Sulfur-rich polymers with functional linkers for high-capacity and fast-charging lithium–Sulfur batteries, Adv. Energy Mater. 8 (2018) 1802423, <https://doi.org/10.1002/aenm.201802423>.
- [68] J. Balach, T. Jaumann, M. Klose, S. Oswald, J. Eckert, L. Giebeler, Improved cycling stability of lithium–sulfur batteries using a polypropylene-supported nitrogen-doped mesoporous carbon hybrid separator as polysulfide adsorbent, J. Power Sources 303 (2016) 317–324, <https://doi.org/10.1016/j.jpowsour.2015.11.018>.
- [69] K.S. Rao, D.D. Pathak, B.P. Mandal, S. Kumar, A.K. Tyagi, Polyaniline/rGO/S composite cathode with GO modified separator for lithium sulfur battery: a multipronged approach to tackle the shuttle effect, Mater. Today Commun. 36 (2023) 106708, <https://doi.org/10.1016/j.mtcomm.2023.106708>.